Comparison of power electronics lifetime between vertical- and horizontal-axis wind turbines

Max A Parker[1,*], Conaill Soraghan[2], Alex Giles[3]

[1]Department of Electrical and Electronic Engineering, University of Strathclyde, Technology and Innovation Centre, 99 George Street, Glasgow, UK, G1 1RD
[2]Offshore Renewable Energy Catapult, Inovo, 121 George Street, Glasgow, UK, G1 1RD
[3]Department of Electrical and Electronic Engineering, University of Strathclyde, Technology and Innovation Centre, 99 George Street, Glasgow, UK, G1 1RD
[*]max.parker@strath.ac.uk

Abstract: A comparison has been made of the power electronics lifetime for 5MW horizontal- and vertical-axis wind turbines, based on dynamic models supplied with generated wind speed time series. Both two- and three-bladed stall-regulated H-rotor vertical-axis turbines were modelled, with several different control parameters. Vertical-axis turbines are likely to lead to a shorter power electronics lifetime as the aerodynamic torque varies with rotor azimuth, leading to a cyclic generator torque, and increased thermal cycling in the power electronics.

An electro-thermal model of a low-voltage converter was created, and used to calculate the switching device temperatures based on the generator torque and speed time series from the turbine model. An empirical lifetime model and rainflow-counting algorithm were used to calculate the lifetime, and this was repeated at different average wind speeds to determine the overall lifetime. The vertical-axis turbine was found to have a lower power electronics lifetime than the horizontal-axis, or require a larger number of parallel switching devices to achieve the same lifetime, although this was lessened by running the turbine with a more relaxed speed control, allowing the rotor inertia to partially absorb the aerodynamic torque ripple. The three-bladed turbine was also found to give a longer power electronic lifetime than the 2-bladed, due to the lower overall torque ripple.

This paper is a postprint of a paper submitted to and accepted for publication in IET Renewable Power Generation and is subject to Institution of Engineering and Technology Copyright. The copy of record is available at IET Digital Library.

1. Introduction

The power electronic converter on a variable-speed wind turbine has been found to be a significant source of turbine failure, although the resulting downtime per failure is low in an onshore turbine, due to the ease with which parts can be replaced [1]. The growing tendency to site turbines off-shore, making access for repairs more difficult means that the converter reliability is becoming increasingly important [2]. As well as conventional horizontal-axis wind turbines (HAWTs), there

is also increasing interest in vertical-axis wind turbines (VAWTs), which could potentially allow significantly larger offshore turbines, reducing the cost of energy [3].

Most wind turbines use converters based on insulated-gate bipolar transistors (IGBTs), which are contained in modules based on one of two types, shown in Figure 1 [4]. The conventional module is used in the low-voltage (<1000V) converters commonly used in wind turbines, and features IGBT and diode chips soldered to copper tracks, which are bonded to a ceramic insulator. Wire bonds connect to the contacts on the tops of the devices. Presspack modules are more commonly used in medium-voltage (>1000V) converters, which are only used in a small number of turbine designs mainly due to higher cost and the existing experience with low-voltage converter designs [5]. These have slightly different degradation mechanisms [6] [7], and will not be considered in this study.

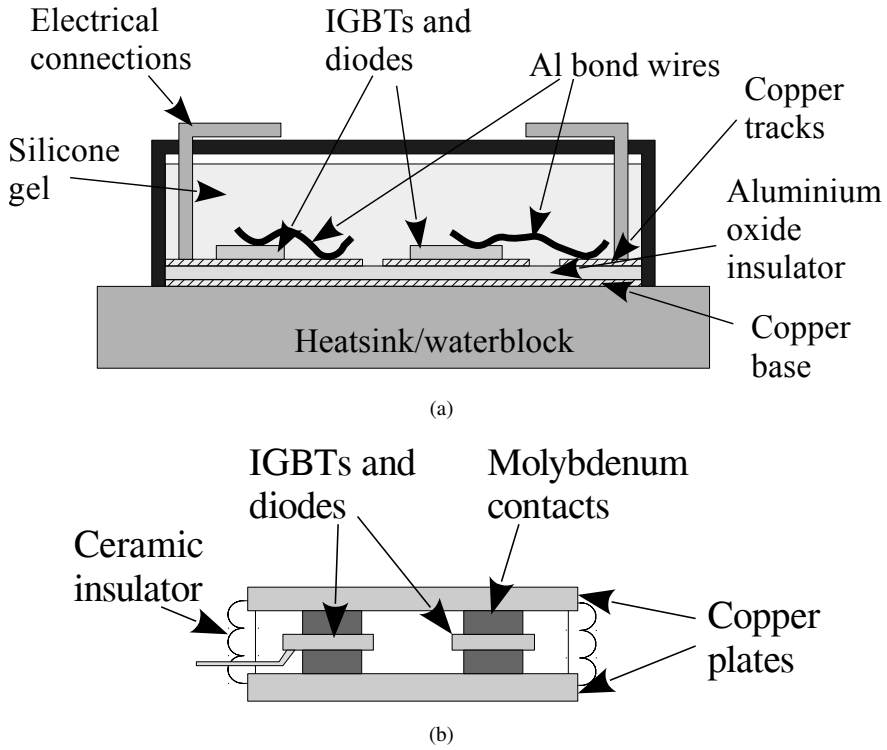

Fig. 1. *Types of IGBT module*
a conventional module
b presspack module

The most predictable degradation mechanisms for power electronics are related to the thermal cycling of the switching devices. Thermal cycling causes fatigue-related damage to the solder attaching the IGBT and diode chips to the copper tracks, and to the join between the aluminium bond wires and the silicon chips, due to the mismatches in the coefficients of thermal expansion of the materials [8]. There is evidence that the main causes of failure of wind turbine converters in service are related to environmental conditions [9], and are less predictable. This is considered to be due to the use of standard converters in a much harsher environment than that which they are designed for, and that converters designed specifically for wind energy applications will reduce these effects.

All previous studies of wind turbine power electronic lifetime have concerned HAWTs, and

are mostly based around doubly-fed induction generators (DFIGs) with part-rated converters [10] [11] [12] [13], with some studies based around generators with fully-rated converters [7] [14] [15], or comparisons with DFIGs [16]. DFIGs have particular issues with thermal cycling as the rotor frequency is very low around the synchronous speed, leading to a high cycle amplitude and reduced lifespan [10]. Turbines with fully-rated converters turbines have the highest rotor frequency at high turbine powers, reducing this effect. While a significant number of DFIG-based turbines are in service, their use in new turbines is being reduced due to difficulties in complying with grid fault ride-through requirements and the increasing use of direct-drive generators, which require a fully-rated converter [5].

In a HAWT, thermal cycling occurs partly due to the alternating current at the converter terminals causing a pulsating loss in the IGBTs and diodes, and partly due to the variations in wind speed leading to a variation in power handled by the converter, resulting in a variation in heating due to the converter losses, and some attempts have been made to quantify the split [11] [16]. In a VAWT, the rotor torque can vary significantly with the rotor position relative to the wind direction, particularly with a two-bladed turbine, which leads to a cyclic torque variation as the turbine rotates. This causes a cyclic temperature variation in the converter in addition to the thermal cycles due to the alternating current and wind speed variation. The result of this is that the converter in a VAWT may have a significantly shorter life than one in a HAWT of similar rating, and the purpose of this study is to quantify the difference in converter life.

2. Model Design

This study builds on previous investigations of the power electronics lifetime of HAWTs [14], and uses a similar methodology. The main difference in methodology is that this study uses turbine models developed in Matlab/Simulink, rather than DNV-GL Bladed in the previous study. The methodology is similar to that used for calculation of turbine blade fatigue lifetime based on time-domain simulation [17].

The model structure is shown in Figure 2. A wind time series is procedurally generated for a given average wind speed and turbulence intensity, and this is fed into a wind turbine model. The turbine model produces a time series of the generator torque and speed, which is used in the electro-thermal model to first calculate the converter current and voltage, then the losses in the switching devices, then the device temperatures. The device temperature time series is used to calculate the converter lifetime for that wind speed, using the lifetime model.

In the wind power spectrum, a spectral gap exists in the region from 1 to 10 cycles per hour, corresponding to periods from 6 minutes to 1 hour [18]. Because of this, fatigue analysis is typically carried out by splitting the wind speed range of the turbine into a number of bins based on the 10-minute average speed, and carrying out simulations of around 10 minutes for each average speed [17]. The results can then be combined to find the overall lifetime based on the proportion of time the average wind speed spends in each bin. In this study, 10-minute procedurally generated wind speed time series were used, as it was desired to determine the effects of the wind speed variability on top of the torque pulsations from the VAWT rotor. Some studies have concentrated either on simulating with a wind time series at a single average speed [7] or across a range of constant wind speeds [12], although others have suggested that the impact of the wind speed variation across the operating range is significant [11].

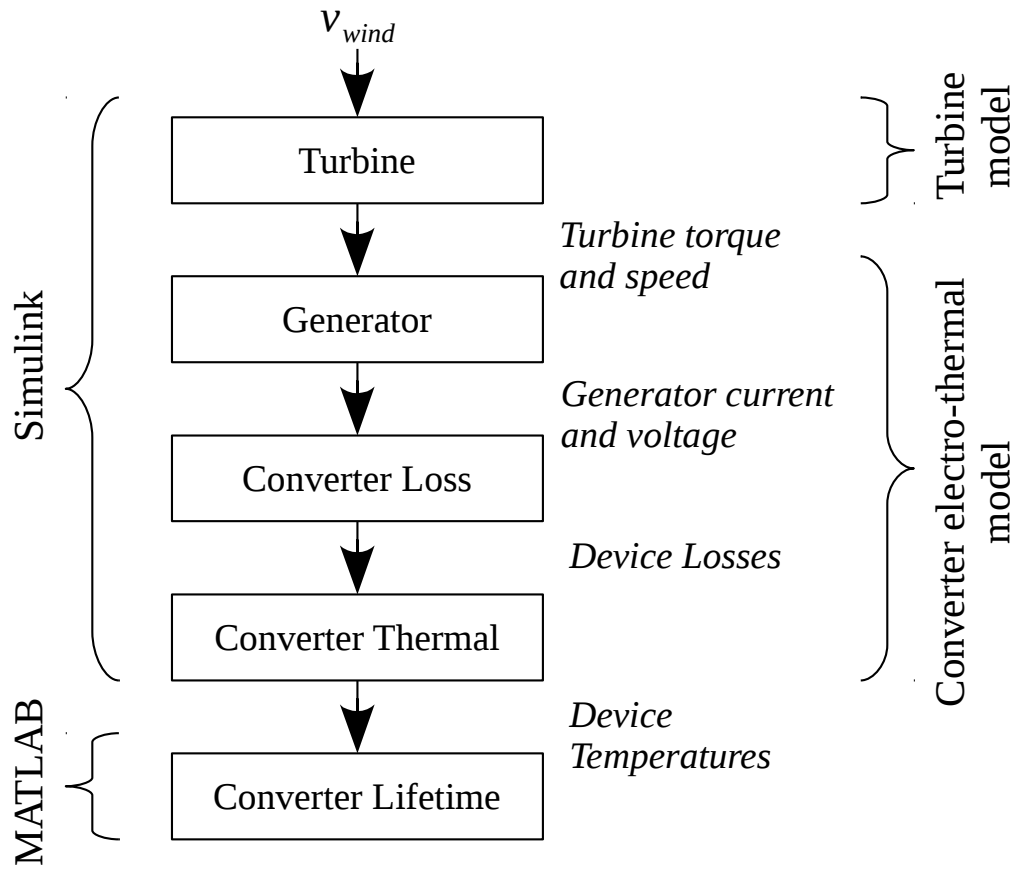

Fig. 2. *Model structure*

2.1. Turbine

For the HAWT, the SUPERGEN 5MW turbine Simulink model was used, which is based on the NREL 5MW reference design [19] with a modified controller design, and this will not be described in depth in this paper. For the VAWTs, 2- and 3-bladed H-rotor turbines were designed using the StrathDMS VAWT model, which is a steady-state model based on blade element momentum theory, with double multiple streamtubes [20] [21]. The StrathDMS results were then incorporated into a pseudo-dynamic turbine model in Simulink, and an appropriate controller designed. The VAWTs were designed to provide a rated power of 5MW at a wind speed of 12m/s, using a chord length of 5m for the 2-blade turbine and 3m for the 3-blade turbine in order to achieve the same peak coefficient of performance for both turbines, at a tip speed ratio of 3.5, and a NACA0012 blade profile was used. Blade parameters for the HAWT are given in reference [19]. The turbine sizes are shown in Figure 3; the VAWT has a larger swept area than the HAWT as VAWTs inherently have a lower aerodynamic efficiency, requiring a larger size to achieve the same rated power.

The turbine models are based around the standard method of using a $C_p - \lambda$ curve, with the mechanical power for the HAWT given by (1), where ρ is the air density, A the swept area of the blades and U_W the wind speed. C_p is the turbine coefficient of performance, which is a function of the rotor tip speed ratio λ and the blade pitch angle β. For the VAWT, the blade pitch is fixed but the rotor torque will vary with the turbine azimuth θ, i.e. as the turbine rotates, as well as with the tip speed ratio, with the mechanical power given by (2). The HAWT aerodynamic torque also

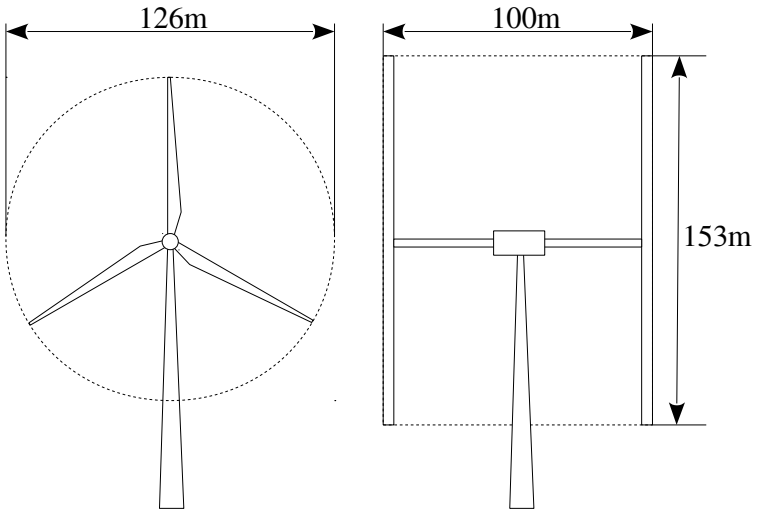

Fig. 3. *Turbines used in this study*

includes a cyclic component, representing the effects of tower-shadowing, but this was found to be largely absent from the generator torque demand due to the action of the turbine controller.

$$P_{mech} = 0.5\rho A U_W^3 C_p(\lambda, \beta) \tag{1}$$

$$P_{mech} = 0.5\rho A U_W^3 C_p(\lambda, \theta) \tag{2}$$

StrathDMS calculates the average aerodynamic torque as the turbine passes through different azimuth ranges, and for different tip speed ratios, and this was used to derive lookup tables for $C_p(\lambda, \theta)$ for the 2- and 3-bladed VAWTs. The lookup table data are plotted in Figure 4. It is immediately clear that the 2-bladed turbine has a greater torque fluctuation with rotor angle, producing two peaks per revolution as the upwind and downwind blades both produce torque peaks at the same azimuth. By contrast, the 3-bladed turbine has a smoother torque, with the peaks from the downwind blades occurring in between those of the upwind ones. In both turbines the torque fluctuation increases at low tip speed ratios, when the blades start to stall for greater proportions of the rotor revolution, and each peak starts to split into two separate peaks. This is a problem when the turbine is operating above the rated wind speed, and stall control is used to limit the turbine power.

The turbine rotation speed, ω, is calculated using (3), where J_{rot} is the turbine inertia, P_{mech} the mechanical power and T_{gen} the torque applied by the generator. A rotor inertia of 2.25×10^8kg m^2 was used, which was estimated in a previous VAWT study.

$$\omega = \frac{1}{J_{rot}} \int \frac{P_{mech}}{\omega} - T_{gen} dt \tag{3}$$

The VAWT is controlled using stall regulation with semi-constant speed control, which uses a proportional-integral (PI) controller to regulate the turbine speed to a reference value. At higher wind speeds, the turbine speed reference is kept at the maximum value, with the turbine power being limited as the turbine operation moves into the stall region. At lower wind speeds, the speed reference tracks the maximum power point line, and is determined from a lookup table of aerodynamic torque vs. speed.

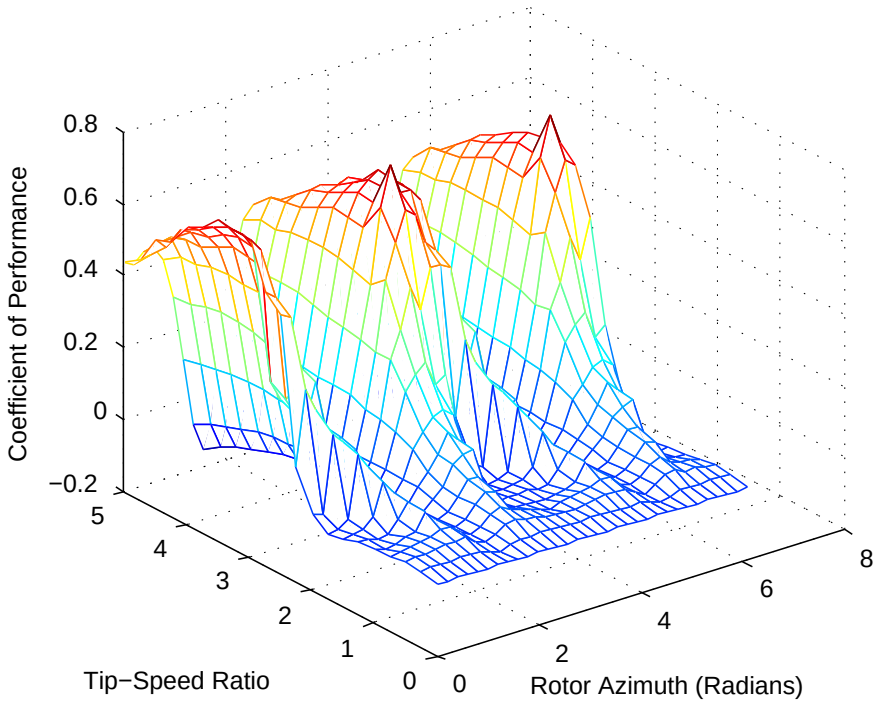

(a)

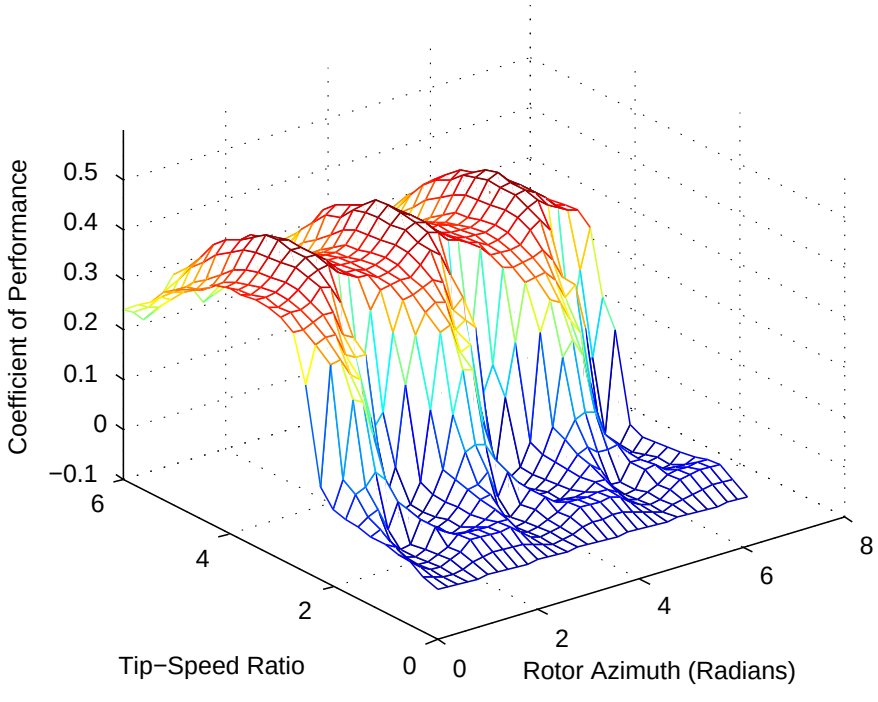

(b)

Fig. 4. *$C_p - \lambda$ curves for the VAWTs*
a 2-bladed
b 3-bladed

The controller diagram is shown in Figure 5. The mechanical torque, $\hat{T}_m$ is estimated from the rate of change of speed and the previously applied electrical torque T_{gen}. This torque will contain ripples, due to the variation in torque with rotor azimuth, and these are filtered using rotational averaging based on the turbine azimuth θ, giving an average torque $\bar{T}_m$. A lookup table is used to find the reference rotor speed $\omega^\star$, and a PI controller used to regulate the actual rotor speed ω via the generator torque demand T_{gen}. It is assumed that the generator torque control bandwidth is sufficiently fast that the generator torque follows the demand exactly.

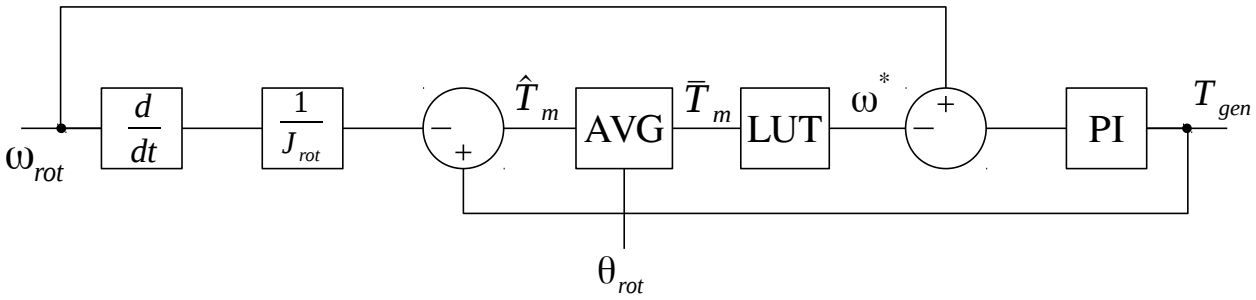

Fig. 5. *VAWT control system*

Control methods are different for the HAWT and VAWTs considered here, with the HAWT being pitch regulated and the VAWTs stall regulated, which may affect the validity of the comparison. However, all the main manufacturers developing HAWTs for offshore use are using pitch regulation, while stall-regulated VAWTs are being considered for offshore use [3]. Furthermore pitch regulation of VAWTs is much less studied, and is mainly concerned with increasing energy capture rather than limiting torque ripple.

2.2. Generator and Converter

For this study, only the generator-side converter was considered. A high speed permanent-magnet generator was used, with a gearbox ratio selected to give rated generator speed at the maximum turbine speed. The generator per-unit reactance is 0.4, and the frequency is 50Hz. Gearbox and generator losses were ignored. The generator terminal voltage magnitude was set to be equal to the electromotive force (EMF), which gives the lowest converter rating for a generator with low inductance [22].

A low voltage converter, with a rated voltage of 690V was used, as that is the most commonly used voltage in large variable-speed wind turbines, and a DC-link voltage of 1300V used. The converter configuration for the generator side is shown in Figure 6, and is based on an integrated power module (IPM) commonly used in wind turbine converters. Each IPM is configured as a half-bridge, requiring a minimum of three for a three-phase converter, and the number of parallel IPMs determines the rating of the converter. A single IPM was modelled, representing one out of the three phases, and the current was obtained by dividing the phase current by the number of parallel IPMs.

2.3. Converter Loss

The converter is modulated using a conventional pulsewidth modulation (PWM) system with third harmonic injection, with a switching frequency of 1kHz. The actual switching was not simulated, as it is assumed to be of a sufficiently high frequency to have no impact on the device temperatures,

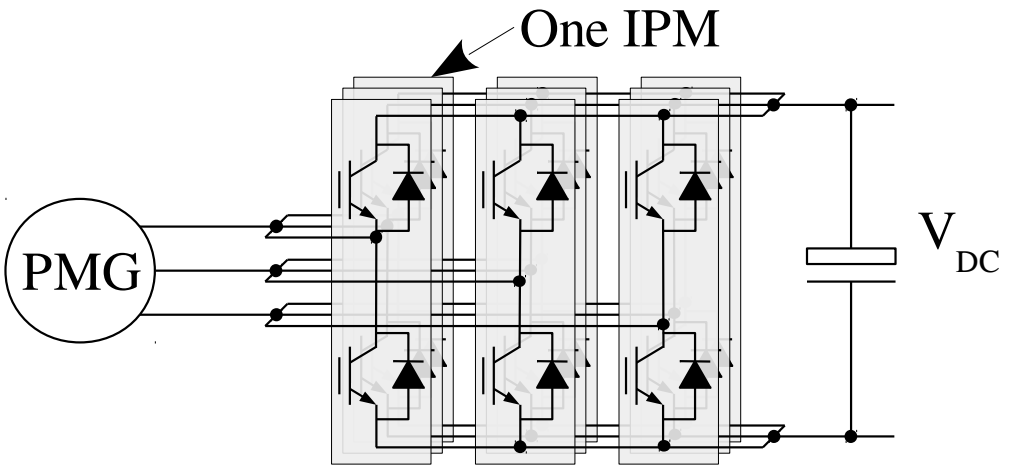

Fig. 6. *Low-voltage generator-side converter configuration*

but the switching frequency determines the switching losses. Losses were calculated according to methods specified by the manufacturer of the IPM, based on the conduction and switching losses for the different devices in the IPM [23]. The effect of the device temperature on these losses was not considered, and the effect on switching loss of having multiple IPMs in parallel was also ignored.

2.4. Converter Thermal

The thermal model for the IPM is provided by the manufacturer [23], and the structure is shown in Figure 7, based on an electrical equivalent circuit. The IGBTs and diodes within the IPM have total losses (conduction and switching) of $P_{tot(T)}$ and $P_{tot(D)}$, and have thermal impedances to the heatsink of $Z_{th(j-s)}$. Each IPM consists of several half-bridge modules connected in parallel, and each half-bridge has multiple diode and IGBT chips in parallel for the high and low side. The thermal coupling between the individual chips within the module itself is considered minimal [23], so all see the same heatsink temperature T_s, and the losses and impedances for all the parallel chips are lumped together. The heatsink to ambient impedance is $Z_{th(s-a)}$, and the heatsink is a water block with a water temperature of 40°C.

The thermal impedance between two points, $Z_{th(1-2)}$ can be modelled in the time domain as a sum of n first order exponential elements given by (4), where R_i and τ_i are the thermal resistance and time constant for each element, which are supplied by the manufacturer. In the manufacturers data, five elements are used for $Z_{th(j-s)}$ and two for $Z_{th(s-a)}$. Equation (4) is Laplace transformed to give (5), which is implemented in Simulink as a sum of continuous transfer functions.

$$Z_{th(1-2)}(t) = \sum_{i=1}^{n} R_i \left(1 - e^{\frac{-t}{\tau_i}}\right) \tag{4}$$

$$Z_{th(1-2)}(s) = \sum_{i=1}^{n} \frac{R_i}{\tau_i} \left(\frac{1}{s + \tau_i^{-1}}\right) \tag{5}$$

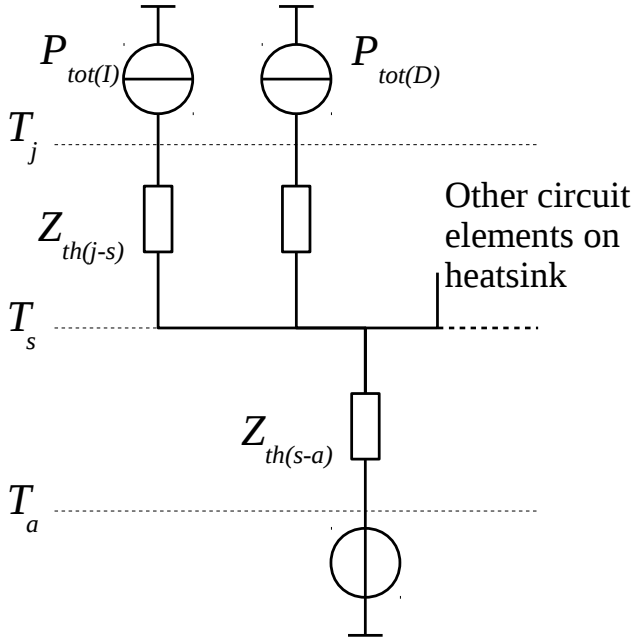

Fig. 7. *IPM thermal model*

2.5. Converter Lifetime

Many methods exist to estimate the lifetime of power electronic devices, but these can be broadly divided into empirical and physical methods [8]. Empirical methods are based on accelerated testing of the devices under a variety of conditions, and fitting the data to a mathematical formula. Physical methods are based on modelling the physical processes which cause the device to fail, and have been shown to be more accurate at predicting the outcome of testing, but require considerable modelling and testing to obtain the parameters of the lifetime model [24] [13]. The empirical methods also require parameters, but these are often supplied by the manufacturers.

Most studies estimate the lifetime using the Coffin-Manson relationship [11] [10] [16], shown in (6), which relates the number of cycles to failure N_f to the junction temperature cycle amplitude ΔT_j, where A and α are constants obtained from accelerated lifetime testing. Other studies are based on the results of the LESIT accelerated lifetime testing, which adds an Arrhenius term to take into account the effects of the mean temperature T_{jm} in K [12] [14], giving the relationship shown in (7), where k_b is the Boltzman constant and E_a the activation energy [25]. This takes into account the effects of the average temperature on the plastic deformation leading to solder fatigue, when operating close to the melting point of the solder.

$$N_f = A\Delta T_j^{\alpha} \tag{6}$$

$$N_f = A\Delta T_j^{\alpha} e^{\left(\frac{E_a}{k_b T_{jm}}\right)} \tag{7}$$

More complex empirical formulae exist, such as the Norris-Landzberg model, which takes cycle frequency into account [6], but the coefficients were not available for the semiconductor device of interest. The Bayerer model is even more complex [26], and coefficients were available from the semiconductor manufacturer, but were only valid for a narrow range of cycle times so this approach

was not used. It has been suggested that thermal cycles of less than 20K will have no effect on solder fatigue, being absorbed by elastic deformation [10]. This is around the maximum for the ripple from the AC waveform in this study, so could be significant, but is not taken into account by the empirical relationships used, so will not be considered.

Whether the mean temperature is taken into account has a significant effect on the results of the lifetime calculations. If the mean temperature is included then the lifetime consumption almost completely occurs at high wind speeds, where the turbine is operating at rated power and the average junction temperature is highest [12] [14]. This is also important for usage in VAWTs, where the higher temperatures at the peaks of the aerodynamic torque will lead to higher lifetime consumption for the temperature ripples from the AC waveform. Lifetime graphs provided by the IPM manufacturer show a dependence on average temperature [23], and were fitted to the LESIT formula to obtain the required constants.

A rainflow counting algorithm was used on the device junction temperature time series, which splits it into multiple representative thermal cycles with different amplitudes and average temperatures [27]. The overall lifetime is estimated from the combination of these cycles using Miner's Rule, shown in (8), where for each cycle i, of a given magnitude and average temperature, the number of cycles is n_i and the number of cycles to failure is N_i. C is a constant, and a value of 1 is usually used.

$$\sum_{i=1}^{k} \frac{n_i}{N_i} = C \tag{8}$$

2.6. Simulation Methodology

The Simulink turbine models were run with multiple procedurally-generated wind time series, with average wind speeds from 4-25m/s with 1m/s steps, representing the operating range of the turbines. A turbulence intesity of 10% was used. The torque and speed time series from the turbine models were used with the electro-thermal model, with each time series run for several different numbers of parallel IPMs. 1,200s of simulation time was used per wind speed, with the first 200s of thermal data discarded as settling time. For each turbine configuration, average wind speed, and number of parallel IPMs, the total lifetime for that wind speed was calculated using the empirical formula and Miner's Rule. The lifetimes from the different wind speeds were combined using Miner's Rule and the probabilities of each average wind speed, calculated using a Rayleigh Distribution with a mean wind speed of 9m/s, typical of an offshore site.

The three turbines are HAWT and 2- and 3-bladed VAWT, with the VAWTs additionally simulated with several controller configurations. Two controller configurations use tight settings for the speed control PI controller, with one introducing a torque limit of 10MNm – without the limit the peak torque can reach up to 40MNm, while the limit is close to the maximum average torque produced by the turbine. This greatly smooths the torque demand, but allows the turbine speed to vary more significantly. A third controller configuration reduces the PI controller coefficients, allowing the turbine speed to vary more, and absorb some of the torque pulsations. In all cases, the minimum generator torque is limited to zero, even though the VAWT rotor may produce negative torque for some ranges of azimuth in certain conditions.

3. Results and Analysis

An example of the generator torque for the VAWTs is shown for the different control parameters, 2- and 3-bladed turbines and at 12 and 22 m/s wind speeds in Figure 8. The torque is normalised by dividing by the average torque at rated turbine power. At 12m/s, the tip speed ratio is around 2.9, which is close to the value for maximum power of 3.5. At 22m/s, the tip speed ratio will be around 1.6, and the splitting of the peaks due to stalling is clearly visible. The 3-bladed turbine shows a significantly lower torque ripple, particularly at 12m/s, while the weak speed control also significantly reduces the ripple.

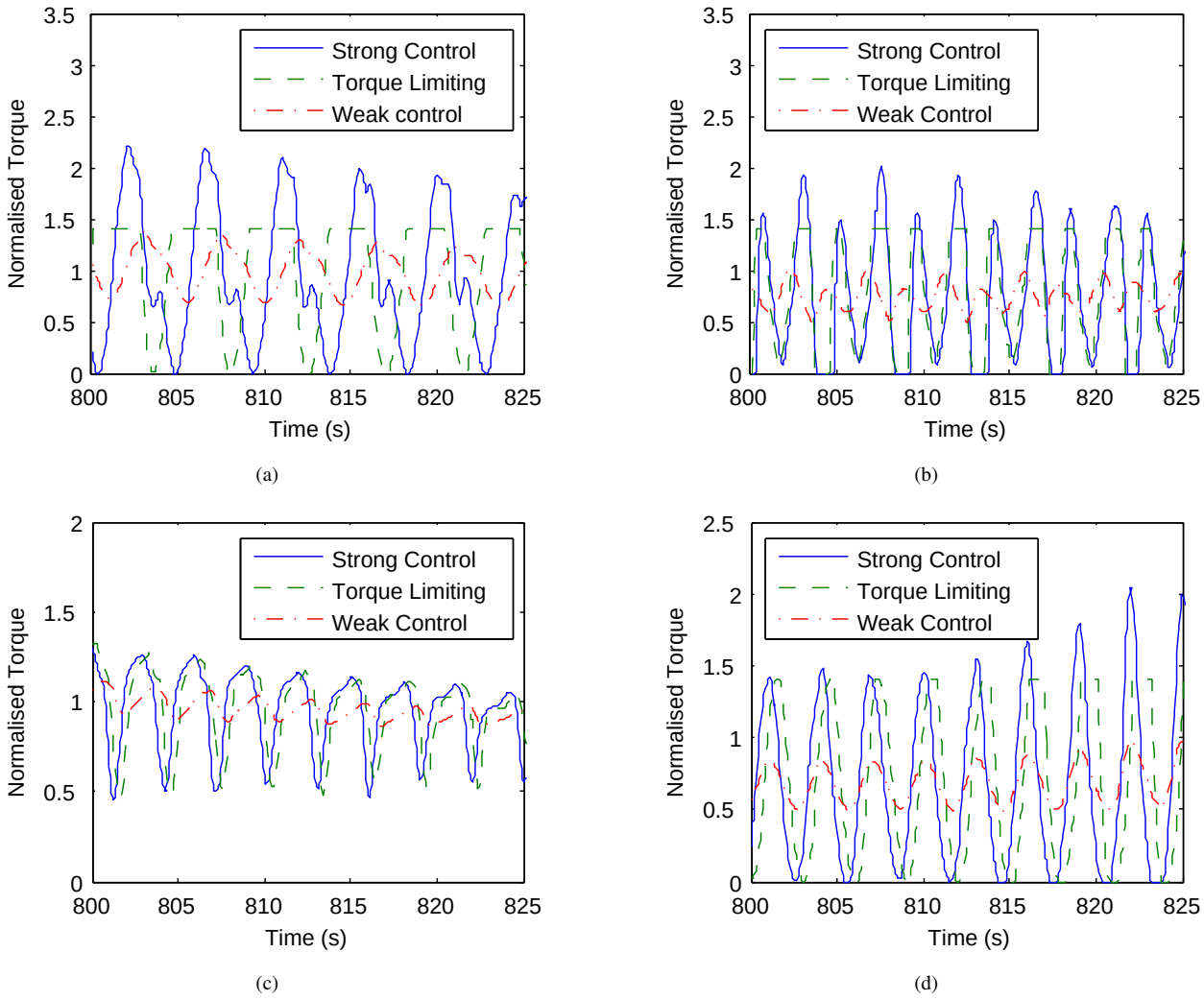

Fig. 8. *Generator torque for:*
a 2-bladed 12 m/s
b 2-bladed 22 m/s
c 3-bladed 12 m/s
d 3-bladed 22 m/s

Using the weaker speed control parameters allows the turbine speed to fluctuate more during a rotation, although this fluctuation was found to be only around 8% of the speed demand, compared

with 2% for the strong speed control parameters. Annual energy extraction for the turbines and control parameters are shown in Table 1, and shows that the control method has a small influence. The 2-bladed turbine has a slightly higher extraction than the 3-bladed, with the HAWT slightly lower, although it should be mentioned that average wind speeds below 6m/s were not simulated for the HAWT due to limitations in the model. This impacts the energy extraction calculations, but it will be shown that this has minimal impact on the lifetime calculations.

Table 1 Turbine annual energy extraction

Turbine/Controller		2-Blade	3-Blade
VAWT	Strong	21.113 GWh	20.577 GWh
	Torque Limiting	21.099 GWh	20.610 GWh
	Weak	21.149 GWh	20.592 GWh
HAWT		-	20.374 GWh

An example of the simulated device temperatures, for the 2-bladed VAWT with strong speed control, is shown in Figure 9 for the 12m/s average wind speed, in the time frame corresponding to that in Figure 8. The temperature cycles due to the cyclic torque are evident, along with the lower amplitude but much higher frequency cycles from the AC generator waveform, which appear as a solid area. The diode has a much higher peak temperature due to having a lower rating than the IGBT, the IPM having been designed for use as an inverter, as opposed to its use here as a rectifier. The construction of the IPM also means that there is limited thermal coupling between the adjacent IGBT and diode chips, which would otherwise tend to equalise their temperatures.

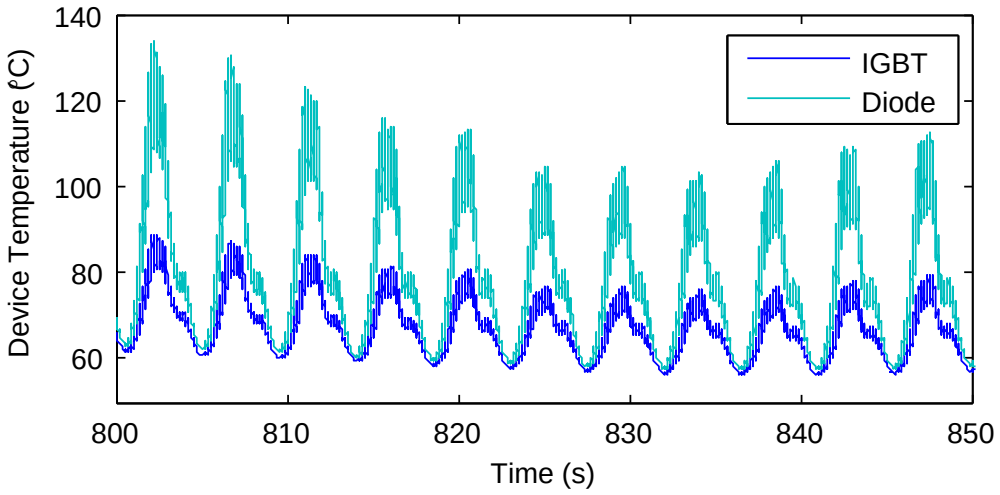

Fig. 9. *Example device temperatures for 2-bladed VAWT with strong speed control*

Lifetime consumption rate is shown against wind speed for the different turbines and control parameters in Figure 10, in which lifetime consumption rate is defined as the probability of the average wind speed being within that bin divided by the lifetime for the bin. For all cases, six parallel IPMs are used. This tends to peak at around rated wind speed, which has a combination of highest power output and higher occurrence. Higher wind speeds will result in higher damage, but are less common. 3-bladed turbines show reduced lifetime consumption than 2-bladed, and weak speed control also reduces the lifetime consumption significantly, with torque limiting having a smaller effect.

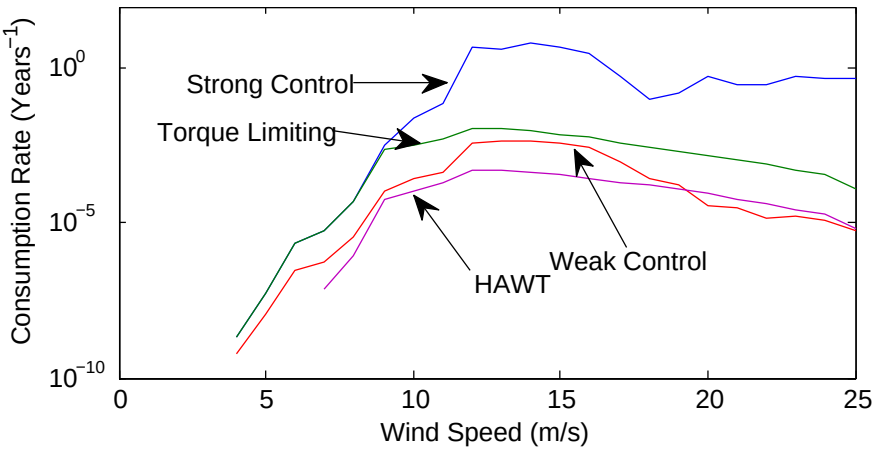

(a)

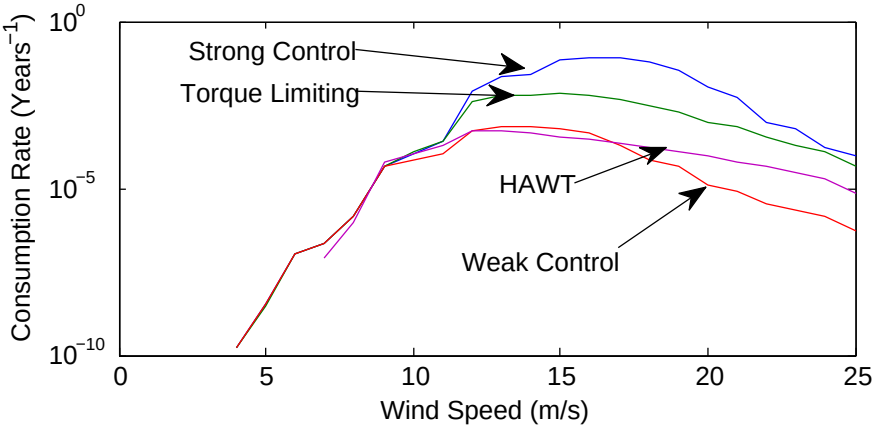

(b)

Fig. 10. *Lifetime consumption rate for 6 parallel IPMs*
a 2-blade
b 3-blade

At high wind speeds, the HAWT torque will be kept constant, and the power regulated with pitch control, so the lifetime consumption will be dominated by the effects of the AC frequency [13]. At low wind speeds, the lower average temperature means that lifetime consumption is low in all turbines. Around the rated wind speed, the HAWT will be switching between power tracking and constant torque modes depending on wind speed, so will experience the highest level of wind-induced thermal cycling.

The variation of lifetime with the number of parallel IPMs (and hence converter rating) is shown in Figure 11, where the dashed line indicates the 20-year turbine lifetime. From these results, the number of parallel IPMs for a 20-year lifetime was interpolated for the different turbine configurations and controllers, and this is given in Table 2. In this table the number of parallel IPMs have been adjusted to take account of the differences in annual energy capture shown in Table 1, in order to allow a fairer comparison between turbines.

Increasing the number of parallel IPMs significantly increases the lifetime in all cases, by reducing the average temperature. For all control parameters, the 3-bladed VAWT requires fewer IPMs for a given converter lifetime than the 2-bladed, but only with weak speed control can the

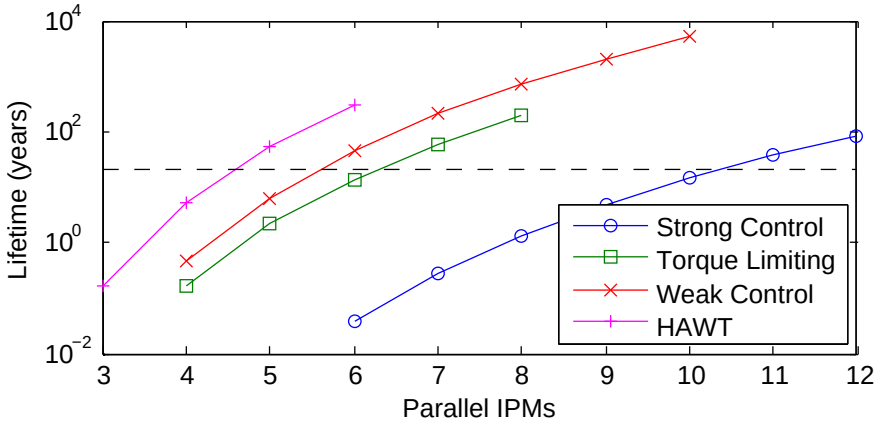

(a)

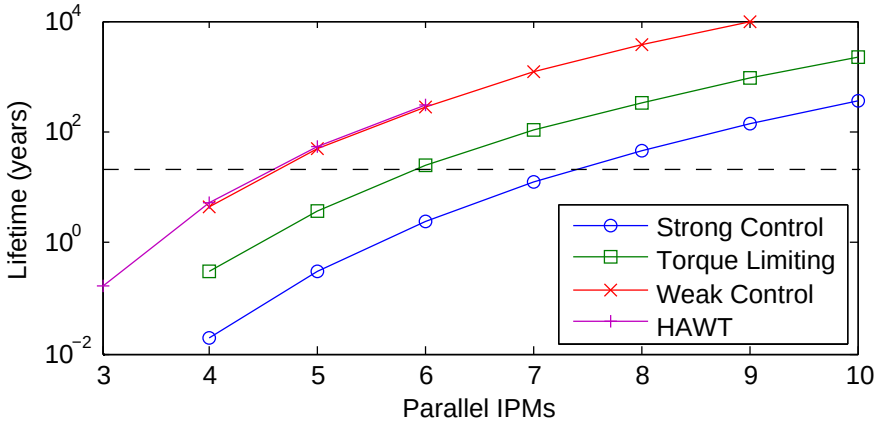

(b)

Fig. 11. *Total lifetime vs. parallel modules, dashed line indicates 20-year target*
a 2-blade
b 3-blade

3-bladed VAWT approach the converter lifetime of the HAWT. Torque limiting results in a slightly lower lifetime than weak speed control, but significantly greater than strong speed control.

The cycles from the rainflow count can be divided into different categories based on the cycle length, and the proportion of damage from each category calculated. In all cases, significant peaks were found around the AC frequency of the generator, around 50Hz, so cycles with a time period of below around 30ms were counted as AC frequency. For the VAWTs, areas of significant damage were found around the two times the rotational period of the turbine in the case of the 2-bladed turbine, and 3 times in the case of the 3-bladed, as well as higher frequencies. To capture these, cycles with a period between 30ms and 8s were counted as rotational ripple. Longer periods, up to the limit of the 1000s simulation duration, were counted as being due to the wind variation. For the HAWT, ripple was observed in the torque demand at three and six times the rotation frequency, but this was extremely small as the turbine pitch system is designed to minimise ripple caused by tower shadowing, and the torque control to avoid responding to these frequencies. For this reason all ripple with a period longer than 30ms was counted as being due to wind variation.

Relative damage from the different components is shown in Figure 12. For the HAWT, damage

Table 2 Parallel IPMs for 20-year lifetime (adjusted for annual energy capture differences)

Turbine/Controller		2-Blade	3-Blade
VAWT	Strong	9.98	7.28
	Torque Limiting	6.01	5.81
	Weak	5.35	4.55
HAWT		-	4.53

mostly comes from the AC frequency time periods, as the generator torque is kept almost constant when the turbine is operating at rated power, where most of the damage occurs. For the VAWTs, strong speed control generally results in the highest contribution from wind variation and to a lesser extent rotational ripple, as the torque is controlled aggressively to maintain a constant speed. Torque-limiting operation also results in a high contribution from rotational ripple, but much lower from wind variation. All the VAWT control methods feature a much higher damage from wind variation than the HAWT, which is due to the use of stall regulation to limit the turbine power.

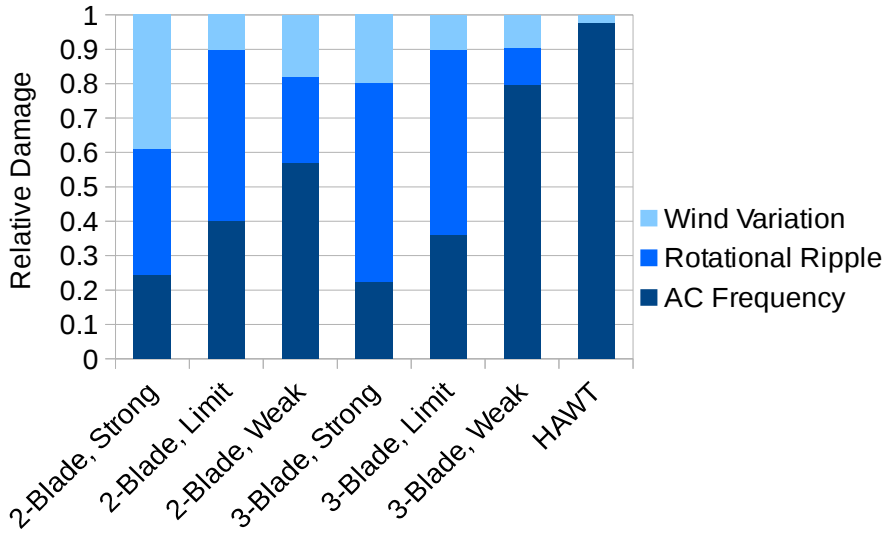

Fig. 12. *Relative damage from different cycle components.*

Attributing damage to the different cycle time ranges in this manner is not entirely accurate. This is because lower frequency cycles will cause the higher frequency cycles to occur at different average temperatures, affecting the damage caused. Due to the exponential relationship between damage rate and average temperature, this will increase the damage from the high frequency cycles compared with having a constant average temperature. This result is important, as one method which has been proposed to reduce the impact of thermal cycles is to deliberately alter the semiconductor switching to increase losses at times when the converter power is lower, to keep the temperature at a more constant but higher level [28]. The results of this study suggest that this would increase the damage from the AC frequency ripple, leading to a lower overall lifetime. However, this depends on the accuracy of the lifetime model, with other lifetime models having a reduced influence from low-amplitude high-frequency cycles [6]. In any case, it is the diode component of the rectifier IPM which limits the lifetime, for which losses are more difficult to deliberately control.

4. Conclusion

Power electronic lifetime has been calculated for stall-regulated vertical-axis wind turbines with 2 and 3 blades and several different control parameter sets, and pitch-regulated horizontal-axis wind turbines, based on thermal cycling in the rectifier switching devices. This study has shown that VAWTs will have a shorter power electronic lifetime compared with HAWTs of similar rated power, or require a significantly higher converter rating to achieve the same lifetime. Damage was found to occur mainly at and above rated power, when the average switching device temperatures are highest. This is due to the strong dependence of the lifetime consumption on average temperature.

The lower lifetime for the VAWTs compared with the HAWT is down to a combination of thermal cycling due to rotational variation in aerodynamic torque and the variations in torque with wind speed. The HAWT has minimal rotational variations, and above rated power will operate with a constant generator torque demand, with the turbine speed controlled using pitch regulation. Above rated power, the VAWTs are regulated in a constant-speed mode, and reducing the bandwidth of the speed controller allows the turbine speed to vary more, reducing the torque variation and increasing the power electronic lifetime significantly. This is particularly the case at higher wind speeds, where the blades are stalling for a significant part of each revolution, and the aerodynamic torque peaks are extremely high relative to the mean value.

A 3-bladed VAWT has lower rotational torque ripples than a 2-bladed one, resulting in longer power electronic lifetime, and when using weak speed control, the lifetime approaches that of the HAWT. The greater speed variation with the weaker controller was found to have negligible effect on annual energy capture, but stronger speed control may be desirable for blade lifetime – the controllers used in this study take no account of the requirements of the mechanical components. Furthermore, two blades may be more desirable for mechanical and manufacturing reasons.

5. References

[1] F. Spinato, P. J. Tavner, G. J. W. van Bussel, and E. Koutoulakos, "Reliability of wind turbine sub-assemblies," *IET Renewable Power Generation*, vol. 3, no. 4, pp. 387–401, 2009.

[2] G. J. W. van Bussel and M. B. Zaaijer, "Reliability, availability and maintenance aspects of large-scale offshore wind farms, a concepts study," in *IMarEst, MAREC conference*, Newcastle Upon Tyne, Mar. 2001.

[3] A. Shires, "Design optimisation of an offshore vertical-axis wind turbine," *Proc. ICE – Energy*, vol. 166, no. EN1, pp. 7–18, 2013.

[4] R. Zehringer, A. Stuck, and T. Lang, "Material requirements for high-voltage high-power IGBT devices," *Solid State Electronics*, vol. 42, no. 12, pp. 2139–2151, 1998.

[5] F. Blaabjerg, M. Liserre, and K. Ma, "Power electronic converters for wind turbine systems," *IEEE Trans. Ind. Appl.*, vol. 48, no. 2, pp. 708–719, 2012.

[6] C. Busca, R. Teodorescu, F. Blaabjerg, S. Munk-Nielsen, L. Helle, T. Abeyasekera, and P. Rodriguez, "An overview of the reliability prediction related aspects of high power IGBTs in wind power applications," *Microelectronics Reliability*, vol. 51, pp. 1903–1907, 2011.

[7] O. Senturk, L. Helle, S. Munk-Nielsen, P. Rodriguez, and R. Teodorescu, "Electro-thermal modelling for junction temperature cycling-based lifetime prediction of a press-pack IGBT 3L-NPC-VSC applied to large wind turbines," in *IEEE Energy Conversion Congress and Exposition*, 2011, pp. 568–575.

[8] S. Yang, D. Xiang, A. Bryant, P. Mawby, L. Ran, and P. Tavner, "Condition monitoring for device reliability in power electronic converters: A review," *IEEE Trans. Power Electron.*, vol. 25, no. 11, pp. 2734–2752, 2010.

[9] K. Fischer, T. Stalin, J. Wenske, G. Wetter, R. Karlsson, and T. Thiringer, "Field-experience based root-cause analysis of power-converter failure in wind turbines," *IEEE Trans. Power Electron.*, vol. 30, no. 5, pp. 2481–2492, May 2015.

[10] M. Bartram, J. von Bloh, and R. W. De Doncker, "Doubly-fed-machines in wind-turbine systems: is this application limiting the lifetime of IGBT-frequency-converters?" in *Power Electronics Specialist Conference, 35th IEEE Annual (PESC 04)*, 2004.

[11] D. Weiss and H.-G. Eckel, "Fundamental frequency and mission profile wearout of IGBT in DFIG converters for windpower," in *Power Electronics and Applications (EPE), 2013 15th European Conference on*, 2013.

[12] F. Fuchs and A. Mertens, "Steady state lifetime estimation of the power semiconductors in the rotor side converter of a 2mw dfig wind turbine via power cycling capability analysis," in *Power Electronics and Applications (EPE2011), Proceedings of the 14th European Conference on*, 2011.

[13] M. Musallam and C. M. Johnson, "Impact of different control schemes on the life consumption of power electronic modules for variable speed wind turbines," in *Power Electronics and Applications (EPE 2011), 2011 14th European Conference on*, 2011.

[14] K. Givaki, M. Parker, and P. Jamieson, "Estimation of the power electronic converter lifetime in fully rated converter wind turbine for onshore and offshore wind farms," in *Proc. IET Power Electronics, Machines and Drives (PEMD2014)*, 2014.

[15] A. Isidori, F. M. Rossi, F. Blaabjerg, and K. Ma, "Thermal loading and reliability of 10-MW multilevel wind power converters at different wind roughness classes," *IEEE Trans. Ind. Appl.*, vol. 50, no. 1, pp. 484–494, Jan. 2014.

[16] D. Weiss and H.-G. Eckel, "Comparison of the power cycling stress of IGBT in DFIG and full size converter for windenergy applications," in *Power Electronics and Applications (EPE'14-ECCE Europe), 2014 16th European Conference on*, 2014.

[17] T. Burton, D. Sharpe, N. Jenkins, and E. Bossanyi, *Wind Energy Handbook*. John Wiley & Sons, Ltd., 2001, ch. 5.

[18] I. Van der Hoven, "Power spectrum of horizontal wind speed in the frequency range of 0.0007 to 900 cycles per hour," *Journal of Meteorology*, vol. 14, no. 2, pp. 160–164, 1957.

[19] J. Jonkman, S. Butterfield, W. Musial, and G. Scott, "Definition of a 5-MW reference wind turbine for offshore system development," National Renewable Energy Laboratory (NREL), Tech. Rep., 2009.

[20] C. Soraghan, W. Leithead, H. Yue, and J. Feuchtwang, "Double multiple streamtube model for variable pitch vertical axis wind turbines," in *43rd AIAA Fluid Dynamics Conference and Exhibition*, 2013.

[21] L. Paraschivoiu, "Double-multiple streamtube model for studying vertical-axis wind turbines," *Journal of Propulsion and Power*, vol. 4, no. 4, pp. 370–377, 1988.

[22] A. Grauers and P. Kasinathan, "Force density limits in low-speed PM machines due to temperature and reactance," *IEEE Trans. Energy Convers.*, vol. 19, no. 3, pp. 518–525, 2004.

[23] A. Wintrich, U. Nicolai, W. Tursky, and T. Reimann, "Application manual – power semiconductors," SEMIKRON International GmbH, Tech. Rep., 2011.

[24] C. Y. Yin, H. Lu, M. Musallam, C. Bailey, and C. M. Johnson, "A prognostic assessment method for power electronic modules," in *Electronic Systems-Integration Technology (ESTC), IEEE Conf. On*, 2008.

[25] W. Wu, P. Held, P. Jacob, and A. Birolini, "Investigation on the long term reliability of power IGBT modules," in *Proc. Int. Simp. Power Semiconductor Devices*, 1995.

[26] R. Bayerer, T. Herrmann, T. Licht, J. Lutz, and M. Feller, "Model for power cycling lifetime of IGBT modules – various factors influencing lifetime," in *Integrated Pwer Systems (CIPS), 5th Int. Conf. On*, 2008.

[27] A. Nieslony, "Determination of fragments of multiaxial service loading strongly influencing the fatigue of machine components," *Mechanical Systems and Signal Processing*, vol. 23, no. 8, pp. 2712–2721, 2009.

[28] D. A. Murdock, J. E. Ramos Torres, J. J. Connors, and R. D. Lorenz, "Active thermal control of power electronic modules," *IEEE Trans. Ind. Appl.*, vol. 42, no. 2, pp. 552–558, 2006.